Comparison of Non-Electric Vehicle Crashworthiness in Crash Tests with Electric Vehicles

Kathy Tang, Suzanne Tylko, Alain Bussières

Abstract This study compares the responses of anthropomorphic test devices (ATDs) in the front and rear seats of an internal combustion engine (ICE) vehicle when impacted by two different bullet vehicles: an electric vehicle (EV) and a comparable non-EV. Five pairs of moving car-to-moving-car side impact tests were conducted with bullet and target vehicle velocities of 48 km/h and 24 km/h, respectively, and ten pairs of moving car-to-moving-car frontal 40% offset tests were conducted at 48 km/h. In both configurations, pairs of same-model ICE vehicles were struck by an EV bullet in one test and a non-EV bullet in the second test. THOR, Hybrid III, or WorldSID ATDs, and child ATDs were placed in front-row and rear seats.

In side impact, responses were scattered. Driver abdominal responses measured an increase in either peak magnitude or loading duration in vehicles struck by EVs. Peak excursion of the far-side rear ATD occurred earlier when the bullet vehicle was an EV, and head responses were dependent on the struck-side occupant. In frontal offset pairs, ATD responses were mixed. The variability of individual paired differences was high in both crash configurations, suggesting that differences in bullet vehicle powertrain alone did not account for the range of paired differences observed.
Keywords car-to-car crash tests, crashworthiness, electric vehicles, frontal impact, side impact

I. INTRODUCTION

A research crash test programme was initiated in 2013 by Transport Canada to investigate the crashworthiness of hybrid, hybrid electric, plug-in hybrid electric, and all-electric vehicles. In frontal crash tests, self-protection in hybrid, hybrid electric, plug-in hybrid electric, and all-electric models was found to be as good as or better than protection in ICE model equivalents [1]. As the market penetration of EVs increased, concerns about the potential incompatibility of these heavier vehicles began to emerge, particularly with respect to the risks posed to occupants of vehicles struck by EVs [2].

Compatibility between vehicles particularly as it pertains to differences in mass, vehicle stiffness, and bumper height has been the subject of numerous studies since at least the 1980s [3]-[13]. Transport Canada participated in and contributed to the International Harmonized Research Activities (IHRA). This voluntary group, led by the National Highway Traffic Safety Administration (NHTSA), conducted harmonized research studies to develop a global regulation for vehicle-to vehicle side-impact protection and frontal compatibility. The work led to a memorandum of understanding between Canada and vehicle manufacturers in 2003 [14].

An updated field study was recently conducted to investigate partner protection for a newer vehicle fleet [15]. The influence of mass, height of the centre of gravity (CG), and stiffness metrics (partner protection metrics, PPMs) on the odds of injury in front-to-side and front-to-front collisions was investigated. PPMs were derived from the results of US New Car Assessment Program (NCAP) and Insurance Institute for Highway Safety (IIHS) frontal crash tests. In both front-to-side and front-to-front collisions, increased odds of injury were associated with increasing partner vehicle mass and energy-equivalent stiffness (KW400), while decreasing odds were associated with increasing maximum displacement of the partner vehicle. In front-to-front impacts, a higher partner vehicle CG was also associated with increased odds of injury. The authors concluded that mass incompatibility was a dominant predictor of injury outcome, and noted that the effect of mass increase associated with EVs may only partially be offset by their lower CGs. The study investigated the effects of all vehicles without specifically comparing EVs to ICE vehicles.

Muller et al. [16] compared the masses, geometries, and stiffness metrics of EVs to those of ICE vehicles using data derived from US NCAP frontal crash tests. While maximum force was greater, dynamic crush was greater, and centre force was lower for EVs than for ICE, EVs were not found to be more aggressive than ICE vehicles in

K. Tang (+1 450-430-7981 ext.184; kathykaixi[dot]tang[at]tc.gc.ca) is a PhD Candidate at the University of Waterloo, Canada and a Research Assistant at Transport Canada. S. Tylko is Chief of Crashworthiness Research at Transport Canada. A. Bussières is head of the crash lab at PMG Technologies

terms of the stiffness metrics studied.

These two studies, Muller et al. [16] and Brumbelow [15], were based on analyses of single vehicle crash tests and field data. The objective of this study was to conduct frontal and side impact moving car-to-car crash tests where the bullet vehicle is an EV or an equivalent model non-EV; and to examine the responses of ATDs placed in front and rear seating locations of the target ICE vehicles.

II. METHODS

Crash Configurations

This study examines the vehicle and ATD responses of the target vehicles in side impact tests (Fig. 1A) and frontal offset tests (Fig. 1B). The test sample consisted of five pairs of car-to-car side impact tests and ten pairs of car-to-car frontal offset tests. Target and bullet vehicle models and test mass differences are presented as a function of test configuration in Table I. The target vehicles selected were chosen to reflect the mix of vehicles typically seen on Canadian roadways and therefore included a mix of model types (SUV, crossover, sedan, and minivan), fabrication dates, and accrued mileage. In pairs where an EV model lacked a corresponding ICE variant, a substitute ICE vehicle was selected based on comparable vehicle height to ensure bumper alignment while targeting a substantial mass differential.

In the side impact tests, target vehicles moving at 24 km/h were struck by bullet vehicles moving perpendicularly to the target at 48 km/h. Target vehicles were struck on the driver side, with the impact point calculated as per the CMVSS 214 procedure. In each pair of side impact tests, the target vehicles were ICE vehicles of the same model, and the bullet vehicle was an EV in one test and an ICE vehicle in the other test.

In the car-to-car frontal offset tests, the two vehicles were each accelerated to 48 km/h with 40% overlap between the vehicles. Overlap was calculated as 40% of the width of the narrower vehicle. In each pair of frontal offset tests, the target vehicles were ICE vehicles of the same model, and the bullet vehicle was an EV in one test and a non-EV (hybrid or ICE) in the other test.

Fig. 1. Schematic of crash configurations: side impact (left), frontal offset (right).

TABLE I

TEST MATRIX. A POSITIVE BULLET-TARGET MASS DIFFERENCE INDICATES THAT THE BULLET WAS HEAVIER THAN THE TARGET. MASS DIFFERENCES NORMALIZED BY THE MASS OF THE HEAVIEST VEHICLE (3368 KG) ARE GIVEN IN PARENTHESES.

Pair #	Crash configuration	Target vehicle	Bullet vehicle (vehicle type)	Bullet-target mass difference [kg]	EV bullet-ICE bullet mass difference [kg]
1	Car-to-car side	2024 Chevrolet Trailblazer	2024 Ford F150 Lightning (EV)	1680 (0.50)	565 (0.17)
			2021 Ford F150 (ICE)	1113 (0.33)	
2		2024 Toyota Corolla Cross	2024 Chevrolet Blazer EV	958 (0.28)	485 (0.14)
			2024 Chevrolet Blazer ICE	479 (0.14)	
3		2022 Nissan Kicks	2025 Hyundai Kona EV	505 (0.15)	334 (0.10)
			2024 Hyundai Kona ICE	172 (0.05)	
4		2024 Honda CRV	2024 Cadillac Lyriq (EV)	910 (0.27)	692 (0.21)
			2014 Toyota Venza (ICE)	224 (0.07)	
5		2025 Hyundai Elantra	2021 Polestar 2 (EV)	725 (0.22)	821 (0.24)
			2024 Honda Civic (ICE)	-94 (-0.03)	
6	Car-to-car frontal offset	2018-2019 Toyota Camry	2020 Kia Soul EV	15 (0.004)	270 (0.08)
			2020 Kia Soul ICE	-184 (-0.05)	
7		2019 Mazda3	2020 Hyundai Kona EV	372 (0.11)	403 (0.12)
			2019 Hyundai Kona ICE	-23 (-0.01)	
8		2014 Nissan Quest	2023 Ford Transit 150 EV	485 (0.14)	261 (0.08)
			2023 Ford Transit 150 ICE	216 (0.06)	

9	2022 Buick Encore	2021 Volvo XC-40 Recharge (EV) 2021 Volvo XC-40 (ICE)	719 (0.21) 235 (0.07)	485 (0.14)
10	2016 Chevrolet Suburban	2022 Ford F150 Lightning (EV) 2014 Ford F150 (ICE)	312 (0.09) 135 (0.04)	177 (0.05)
11	2021-2022 Mitsubishi Mirage	2015 Nissan Leaf (EV) 2008 Pontiac G5 (ICE)	542 (0.16) 353 (0.10)	194 (0.06)
12	2017-2019 Toyota Corolla	2024 BMW i4 (EV) 2020 Hyundai Ioniq Hybrid	752 (0.22) 159 (0.05)	617 (0.18)
13	2018 Hyundai Elantra GT	2018 Volkswagen e-Golf (EV) 2019 Volkswagen Golf (ICE)	318 (0.09) 65 (0.02)	246 (0.07)
14	2020 Toyota Rav4	2020 Kia Niro EV 2020 Kia Niro Hybrid	219 (0.06) -105 (-0.03)	316 (0.09)
15	2021 Hyundai Venue	2023 Subaru Solterra (EV) 2022 Volkswagen Taos (ICE)	767 (0.23) 288 (0.09)	473 (0.14)

ATD selection and positioning

The tests were conducted over a period of several years and designed for multiple programmes. As a result, while ATDs were always placed in the front and rear outboard seating locations, only those that could be matched (within 10 mm) between target vehicles of the same pair were included in the present study. A "matched pair" of ATDs was defined as a pair of ATDs in the same seating position in a pair of target vehicles of the same model. Examples of ATD installations in the target vehicles are shown in the Appendix.

Side impact target vehicles

ATD type and placement for each matched pair of target vehicles are presented in Table II. The target vehicle driver seats were occupied by a WorldSID 50th percentile male ATD (WS-50). Driver WS-50s in Pairs #1, #2, and #4 were installed as per the NHTSA positioning procedure for the WS-50. In Pair #3, the driver seat track was halfway between the mid and rearmost positions but otherwise installed as per the NHTSA positioning procedure.

A second WS-50 was placed in the front passenger seats. The fore-aft position of the seat was adjusted to be aligned with the driver seat. Other than the seat track position, the front passenger ATD was installed as per the NHTSA positioning procedure.

The two rear outboard seating positions were occupied by child ATDs, including the CRABI 12-month-old (CRABI 12M) installed in rear-facing infant seats, the Q3S installed rear-facing in convertible Child Restraint Systems (CRS), and the Q10 installed in belt-positioning boosters or seated directly on the vehicle seat. In some instances, a foam block was placed behind the Q10 to help obtain a more upright seating posture and to help the lower legs hang freely over the front edge of the seat cushion.

TABLE II

ATDS AND CRS INSTALLED IN EACH PAIR OF TARGET VEHICLES IN SIDE IMPACT TESTS. TABLE IS COLOUR CODED BY ATD STATURE.

Pair #	Driver	Front passenger	Left rear passenger	Right rear passenger
1	WS-50	WS-50	CRABI 12M + Infant seat with base	Q10 + foam block + low-back booster
2	WS-50	WS-50	Q10 + foam block (no booster)	Q10 + high-back booster
3	WS-50	WS-50	Q10 + foam block + low-back booster	Q3S + rear-facing CRS
4	WS-50	WS-50	Q10 (no booster)	n/a
5	WS-50	WS-50	n/a	Q10 + foam block + low-back booster

Frontal offset target vehicles

ATD type and placement for each pair of target vehicles are presented in Table III. The THOR 5th percentile female (TH-05F) lumbar spine was adjusted in the slouched or neutral as indicated in the table. With few exceptions (for example, seat-track position), THOR and Hybrid III ATDs in the front-row seats were installed as per their respective seating procedures. Importantly, ATD positioning was matched (to within 10 mm) between target vehicles of the same pair. Front-row seats occupied by the THOR or Hybrid III 50th percentile male (TH-50M or HIII-50M, respectively) were adjusted to mid or rear-of-mid track positions. Front-row seats occupied by the TH-

05F or Hybrid III 5th percentile female (HIII-05F) were adjusted to the mid track position, with the sole exception of the front passenger seat in Pair #15, which was halfway between the foremost and mid track positions.

Child ATDs (Q6, Q10, or Hybrid III 6-year-old (HIII 6YO)) and 5th percentile female ATDs (TH-05F and HIII-05F) were placed in the second- and third-row seats of the target vehicles. HIII 6YO and Q6 ATDs were installed in forward-facing CRS or booster seats. Q10s were installed in boosters or directly on the vehicle seat.

TABLE III

MATCHED PAIRS OF ATDS IN FRONTAL OFFSET TESTS. TABLE IS COLOUR CODED BY ATD STATURE.

<table>
<tr><th>Pair #</th><th>Driver</th><th>Front passenger</th><th>2nd row left</th><th>2nd row right</th><th>3rd row left</th><th>3rd row right</th></tr>
<tr><td>6</td><td>TH-50M
Rearmost</td><td>HIII-05F + RibEye
Mid</td><td>n/a</td><td>n/a</td><td rowspan="2">n/a</td><td rowspan="2">n/a</td></tr>
<tr><td>7</td><td>TH-50M
¾ track</td><td>HIII-05F + RibEye
Mid</td><td>n/a</td><td>HIII-05F + RibEye</td></tr>
<tr><td>8</td><td>TH-50M
Rearmost</td><td>TH-05F (slouched)
Mid</td><td>Q6
CRS</td><td>n/a</td><td>Q10
Booster</td><td>Q10
Booster</td></tr>
<tr><td>9</td><td>HIII-50M
¾ track</td><td>HIII-50M
Aligned with driver</td><td>Q6
Booster</td><td>Q10
Booster</td><td rowspan="7">n/a</td><td rowspan="7">n/a</td></tr>
<tr><td>10</td><td>HIII-50M
Mid</td><td>HIII-50M
Mid</td><td>n/a</td><td>n/a</td></tr>
<tr><td>11</td><td>TH-50M
¾ track</td><td>TH-05F (slouched)
Mid</td><td>n/a</td><td>Q10
No booster</td></tr>
<tr><td>12</td><td>TH-50M
Mid</td><td>HIII-05F
Mid</td><td>n/a</td><td>TH-05F (slouched)
IIHS procedure</td></tr>
<tr><td>13</td><td>TH-50M
Mid</td><td>HIII-05F
Mid</td><td>HIII 6YO
CRS</td><td>HIII-05F</td></tr>
<tr><td>14</td><td>TH-50M
Mid</td><td>HIII-05F
Mid</td><td>n/a</td><td>HIII-05F + RibEye</td></tr>
<tr><td>15</td><td>TH-50M
Mid</td><td>TH-05F (neutral)
¼ track</td><td>Q10
No booster</td><td>n/a</td></tr>
</table>

Instrumentation

In the side impact tests, tri-axial accelerometers were placed at approximate CG and front and rear right sill beams of the target vehicle. A complete list of instrumentation for all ATDs is provided in Table A I-Table A IV . Notably, the driver WS-50s were instrumented with the RibEye deflection measurement system (Boxboro Systems LLC, Boxborough, MA, USA), which measures deflection in three axes at three location each on the shoulder rib, three thorax ribs, and two abdomen ribs; the WS-50 in the front passenger seat was instrumented with 2D IR-TRACCs, which measures deflection in the fore-aft and lateral directions at the mid location on each rib; and the struck-side Q10 was equipped with the side impact kit, which included the modified shoulder and lateral IR-TRACCs.

In the frontal offset tests, tri-axial accelerometers were placed at each vehicle CG, and uni-axial accelerometers were placed at the base of each B pillar. A complete list of instrumentation for all ATDs is provided in Table A II, Table A V, and Table A VI. In addition to the sternum potentiometer, four pairs of installations of the HIII-05F (two pairs in the front passenger seat, two pairs in the right rear seat) were equipped with the RibEye deflection measurement system to measure the fore-aft and lateral displacement at 12 locations across the thorax.

Pre- and post-test measurements, high-speed video

Pre-test ATD positioning was recorded using a FaroArm Arm 3D metrology system (FARO, Lake Mary, Florida, USA). Positioning was matched to within 10 mm, prioritizing the head CG, H-points, and knee and ankle target locations. In the side impact tests, 3D scans of the struck-side doors and sills of the target vehicles were acquired pre- and post-test to measure vehicle deformations (Creaform 3D, Laval, Quebec, Canada). The 3D scans were acquired with an optical laser-based Coordinate Measuring Machine (CMM) scanner with a volumetric accuracy of 0.078 mm. The same scanner and same settings were used for each scan.

Inboard and off-board cameras (Integrated Design Tools, Pasedena, CA, USA) captured high-speed videos with a frame rate of 1 kHz. In all tests, off-board cameras obtained lateral, oblique, and top views of the vehicles. In the side impact tests, on-board cameras were placed on target vehicles to obtain a view of the B pillar, a view of the front-row centre console, frontal views of the four occupants, and lateral views from the far-side front and rear passenger doors. In the frontal offset tests, onboard cameras were placed to obtain oblique left and right views of the driver, a view centered behind the two front-row seats, a lateral view of the right front passenger, and frontal, oblique, and side views of both rear occupants.

Data analysis

Data preprocessing

ATD kinematic and kinetic data and vehicle acceleration data were recorded at 10 kHz and preprocessed as per SAE J211 [17]. Vehicle acceleration-time responses with signal disruptions, as well as spikes or sudden plateaus in RibEye signals resembling the signal interference reported in [18], were removed from the analysis.

In the side impacts, resultant RibEye deflections recorded by the driver WS-50s were calculated from x-, y-, and z-components. 2D IR-TRACC resultant deflections recorded by the front passenger WS-50s were calculated from x- and y-components. In the frontal impacts, resultant IR-TRACC deflections recorded by the TH-50 and TH-05 were calculated from x-, y-, and z-components.

Paired comparison of vehicle acceleration responses

The vehicle accelerations of target vehicles struck by EV bullets were compared to those struck by non-EV bullets. The vehicle pulse characteristics examined were the peak acceleration, delta V, and average acceleration, all computed from target vehicle lateral accelerations (Ay) in the side impacts and target vehicle fore-aft accelerations (Ax) in the frontal offset tests. Delta Vs were computed as the maximum of the integral of the Ay or Ax-time curve, using the cumulative trapezoid method [19] and a timestep of 0.1 msec. Average Ay and average Ax were computed over the first 100 msec of the impact.

The statistical significance of differences in target vehicle pulse characteristics as a function of bullet vehicle type was determined using the one-sided paired t-test, with α=0.1. For each crash configuration, a total of nine t-tests were conducted (three pulse characteristics computed from accelerations recorded at three locations on the vehicle). For each test, the null hypothesis was that the target vehicle response would not be greater when struck by the EV bullet than when struck by the non-EV bullet. Since multiple t-tests were conducted, the Holm-Bonferroni correction for multiple comparisons was applied [20]. Given m hypothesis tests (in this case, m=9), the Holm-Bonferroni correction is applied by first sorting the p-values in ascending order $p_1, \ldots, p_m$, then rejecting the null hypothesis associated with the k-th p-value p_k if $p_k < \frac{\alpha}{m+1-k}$.

Comparison of sill beam deformations in side impact

In side impacts, the sill beam deformations of target vehicles struck by EVs were compared to those struck by ICE bullets. To compute target vehicle deformations, pre- and post-test scans were superimposed on each other by aligning landmarks in post-processing software (Creaform 3D, Laval, Quebec, Canada). Approximately 15 to 20 landmarks were used per vehicle. The landmarks selected were on the front and rear of the vehicle, and were on areas of the vehicle that were not deformed during the crash. Using the superimposed scans, vehicle deformations were computed as the lateral (y-) distance between pre-test and post-test scans at the same fore-aft (x-) and vertical (z-) positions (InnovMetric Software, Quebec City, Quebec, Canada). Comparisons of the scans did not include the B-pillar due to missing data points.

Analysis of ATD kinematic responses

The “paired difference” in a given ATD kinematic response, defined as the difference in the response within a matched pair of ATDs, was defined to be positive if the response was greater in the vehicle struck by the EV than in the vehicle struck by the ICE bullet. Paired differences ≤5 g or ≤5 mm in magnitude were considered to be within the range of repeatability. For this analysis, the paired difference in driver head 3 ms clip in Pair #3 was excluded because in the vehicle struck by the EV, the peak resultant head acceleration occurred when the WS-50 arm contacted its head, and the contribution of arm contact could not be isolated. Since a mix of different ATDs with different instrumentation were used in each seating position, sample sizes for each ATD were too small for statistical testing. Statistical testing of the aggregate sample was not conducted.

In tests with the TH-50 or TH-05, both the maximum fore-aft deflection (Dx) and C_{max} [21], which is the maximum resultant deflection recorded across all four thorax IR-TRACCs, were computed.

The ATD injury metrics listed in Table A I- Table A IV were computed to identify instances where the Injury Assessment Reference Values (IARVs) [22] were surpassed in the side impacts. Instances of head 3 ms clips exceeding 80 g and chest 3 ms clip exceeding 60 g were also identified.

In preliminary analyses conducted for this study, the relationship between bullet-target mass difference and front-row ATD response in the target vehicle was modeled using linear regression. The results of the linear regression did not yield any notable findings: in the side impact tests, ATD responses were either not well correlated with mass difference ($R^2 < 0.5$) or well below IARVs; in the frontal offset tests, the goodness-of-fit of the linear models were always low ($R^2 < 0.5$). Therefore, the results of the linear regression models are provided in the Appendix but are not discussed further.

III. RESULTS

Side impact

Paired comparison of target vehicle responses

Vehicle pulse characteristics computed from Ay-time responses measured at the target vehicle CG, front right sill beam, and rear right sill beam are presented in Fig. 2 and the Appendix. Statistically significant mean paired differences are indicated by an asterisk (*), while NS indicates that the mean paired difference was not statistically significant. Acceleration-time plots recorded from the target vehicle CGs are provided in the Appendix.

In all pairs, delta V and average acceleration at the vehicle CG and front sill beam were greater for vehicles struck by an EV than for those struck by an ICE bullet. However, after applying the Holm-Bonferroni correction for multiple comparisons, the difference was statistically significant for only the front sill beam delta V and front sill beam average acceleration. All other paired differences in response (i.e., peak Ay at the front sill beam, all vehicle pulse characteristics at the CG and rear sill beam) were not statistically significant.

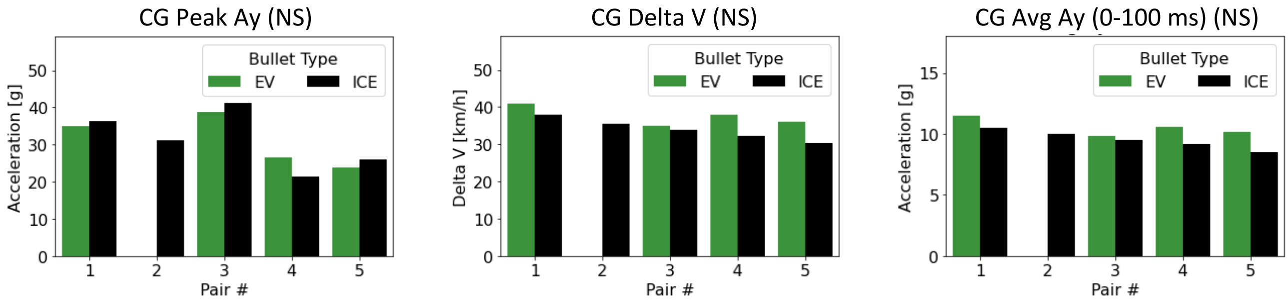

Fig. 2. Peak Ay, delta V and average acceleration computed from Ay-time responses measured at vehicle CGs.

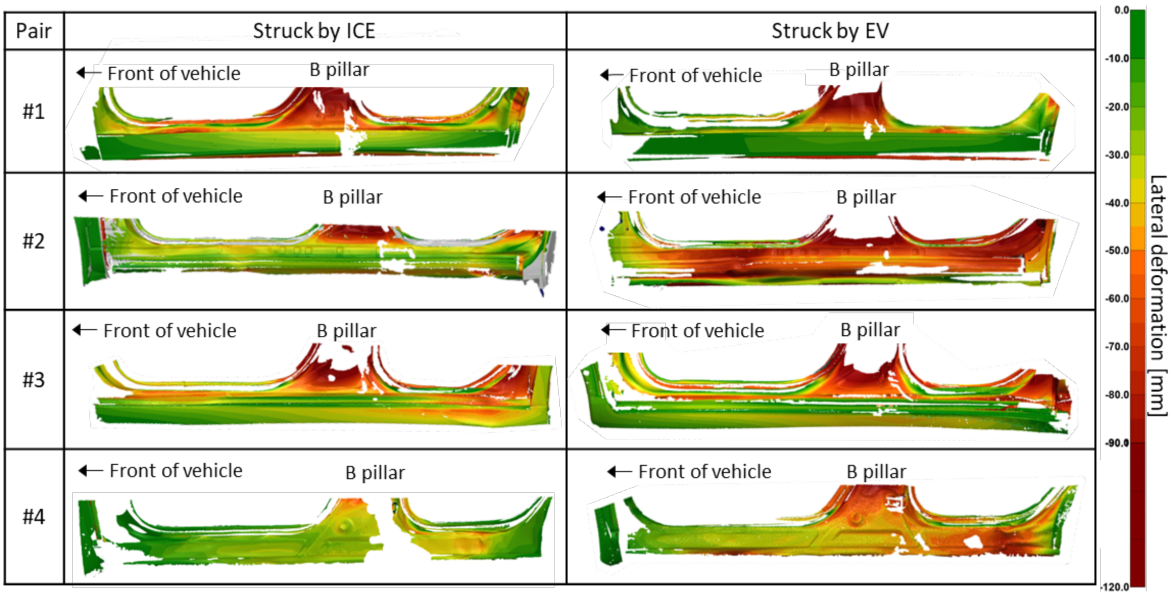

Fig. 3. Heat maps showing deformations of target vehicle sill beams.

Comparisons of target vehicle sill deformations as a function of bullet vehicle type yielded mixed results (Fig. 3). Scans are coloured according to deformation (defined as lateral (y-) distance between pre- and post-test scans at the same fore-aft (x-) and vertical (z-) positions), with deformation increasing from green (≤10 mm deformation) to red (≥ 90 mm deformation). By a qualitative comparison of the colour maps, deformations of the sills in Pair #2 and Pair #4 appeared to be greater when struck by the EV than when struck by the ICE bullet. By contrast, for Pair #1 and Pair #3, the sill appeared to have greater deformations when struck by the ICE bullet than when struck by the EV, especially near the base of the B pillars in Pair #1 and at the rear sills in Pair #3.

Median paired differences in ATD kinematic responses in target vehicles

The analysis included matched pairs of ATDs on both struck and far side. Adult ATDs were always placed in the front-row seats, and pediatric ATDs in the rear seats.

Paired differences in peak head, shoulder, thorax, abdomen, and pelvis kinematic responses were computed for each matched pair of ATDs (Fig. 4). A positive difference indicates that the response was greater in the vehicle struck by the EV than in the vehicle struck by the ICE. The grey shaded region indicates paired differences ≤ 5 g or ≤ 5 mm in magnitude, which were considered to be within the range of repeatability. Markers outside the grey shaded region are annotated according to pair number. The median paired difference, which is less sensitive to outliers than the mean, was computed for each response (Fig. 4, red vertical lines). If the median paired difference of a given response exceeded the range of repeatability, then at least half of the paired differences in the response exceeded the range of repeatability.

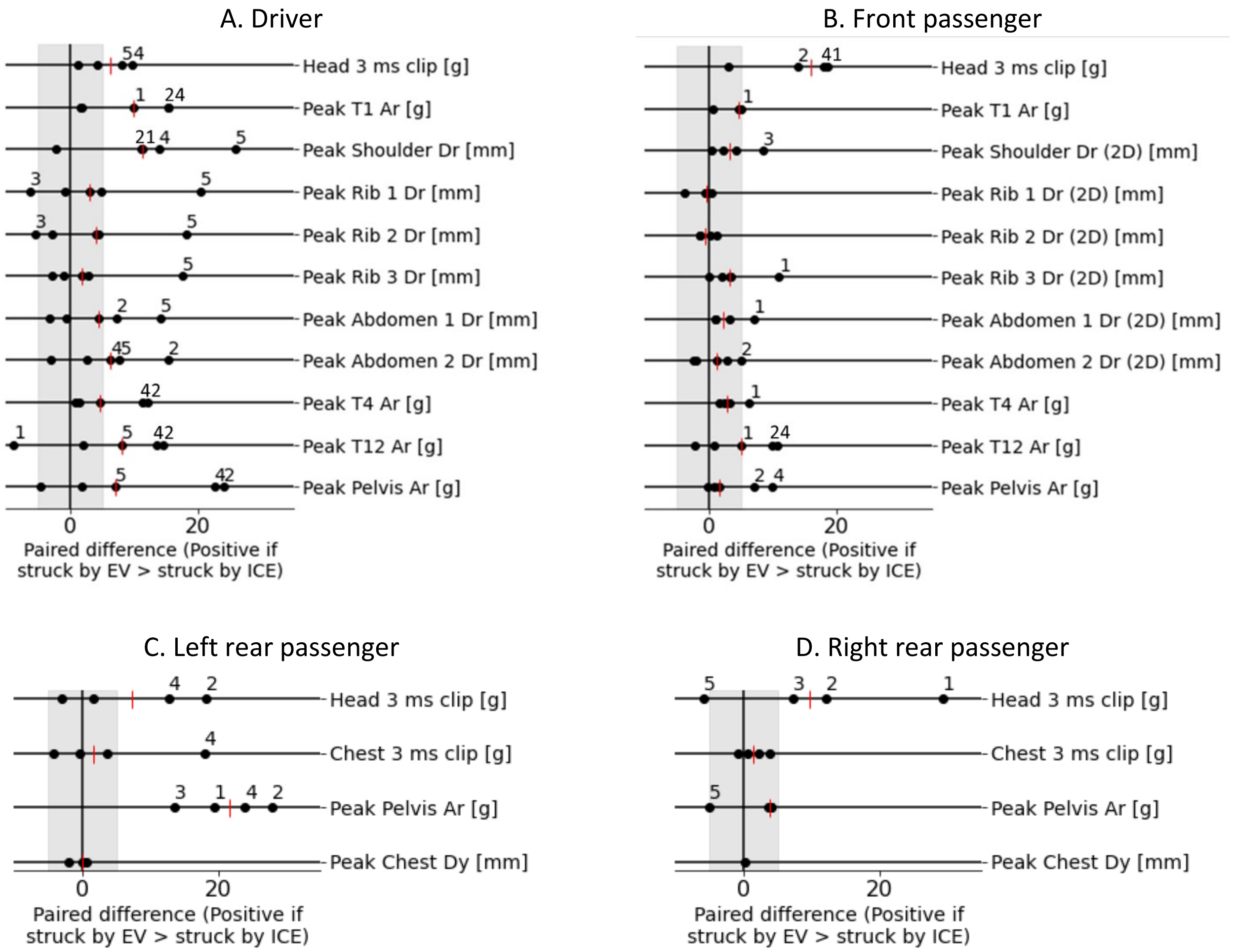

Fig. 4. Paired differences in peak kinematic responses of the ATDs in the target vehicles of side impact crash tests. Ar = resultant acceleration, Dr = resultant deflection, Dy = lateral deflection.

All median paired differences shown in Fig. 4 were either within the range of repeatability or indicated greater responses in vehicles struck by EVs than in vehicles struck by ICE bullets. For the driver ATD (Fig. 4A), head 3 ms clips, peak shoulder and lower abdomen Dr, and peak T1, T12, and pelvis Ar were greater in vehicles struck by EVs than in vehicles struck by ICE bullets. The peak shoulder Dr had the greatest median paired difference in deflection (11 mm), and the peak T1 Ar had the greatest median paired difference in acceleration (10 g). In the left rear seating position (Fig. 4C), head 3 ms clips were 7 g greater and peak pelvis accelerations were 22 g greater in vehicles struck by EVs than in vehicles struck by ICE bullets. For ATDs on the far side (Fig. 4B, D), head 3 ms clips were greater in vehicles struck by EVs than in vehicles struck by ICE bullets (median paired differences of 16 g for the front passenger and 10 g for the right rear passenger).

Examination of individual paired differences in target vehicles

When examining individual matched pairs of ATDs on the struck side, few injury metrics reached or surpassed the IARV or regulatory criteria. In Pair #2, the peak Dy of the driver (WS-50) lower abdomen exceeded the IARV of 39 mm in the vehicle struck by the EV (46 mm) but not in the vehicle struck by the ICE bullet (32 mm, Fig. 5A). In Pair #1, the chest 3 ms clip of the CRABI 12M in the left rear seat exceeded 60 g both in the vehicle struck by the EV and in the vehicle struck by the ICE bullet, but the paired difference (4 g) was within the range of repeatability (Fig. 5B). In Pair #4, the chest 3 ms clip of the Q10 in the left rear seat exceeded 60 g in the vehicle struck by the EV (62 g) but not in the vehicle struck by the ICE bullet (44 g, Fig. 5B).

Differences other than peak magnitude were also observed in the time-varying kinematic responses measured on the struck side. For example, in Pair #1, differences in peak duration were observed in the abdomen and shoulder deflections of the driver ATD (Fig. 6A-B). Differences in peak fore-aft deflection were also observed for the driver WS-50. Pair #5, for example (Fig. 6C), resulted in a 17 mm difference in the peak fore-aft deflection of the Thorax 2 rib.

When examining individual matched pairs of ATDs on the far side, the only injury metric to surpass its IARV or regulatory limit was the head 3 ms clip (Fig. 5C). In Pairs #1 and #5, in both the vehicle struck by the EV and the vehicle struck by the ICE bullet, the Q10 in the right rear seat recorded head 3 ms clips exceeding 80 g. The head of the Q10 was observed in each case to have contacted the CRS on the struck side of the vehicle. In Pair #1, the head 3 ms clip was 29 g greater in the vehicle struck by the EV. In Pair #5, the head 3 ms clip was 6 g greater in the vehicle struck by the ICE.

In Fig. 7, two examples of the excursions of the Q10 on the far side are presented. Panel A shows freeze frames of the Q10 (blue suit) in Pair #2 at the approximate time of peak head excursion. Maximum excursion was reached at 126 ms in the vehicle struck by the EV compared to 138 ms in the vehicle struck by the ICE. The head of the Q10 on the far side (blue suit) contacted the Q10 on the struck side (yellow suit) in the vehicle struck by the EV but not in the vehicle struck by the ICE bullet. Fig. 7B shows freeze frames of the Q10 in Pair #5 at 86 ms, the time at which the Q10 in the vehicle struck by the EV first made contact with the CRS on the struck side. At 86 ms in the vehicle struck by the ICE bullet, the Q10 head has not yet made contact with the CRS on the struck side. Comparing the position of the Q10 head relative to the vehicle head restraints, the head excursion of the Q10 appears to be greater in the vehicle struck by the EV than in the vehicle struck by the ICE bullet.

While none of the injury metrics of the WS-50 in the front passenger seat exceeded IARVs or regulatory limits, contact of the passenger head with the driver was observed in some instances.

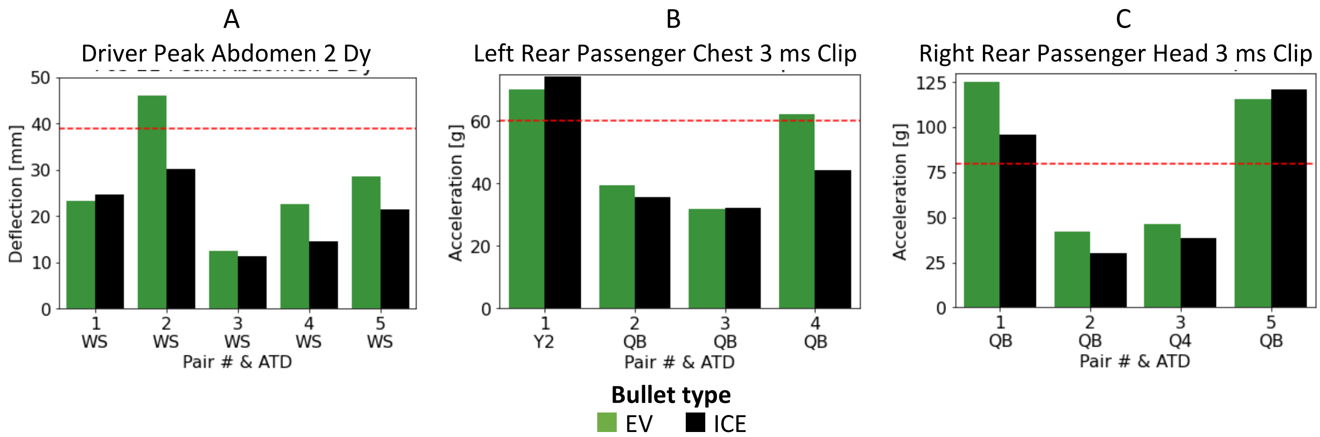

Fig. 5. Injury metrics for which at least one instance of exceeding the reference value was found. The red line indicates the IARV or regulatory limit.

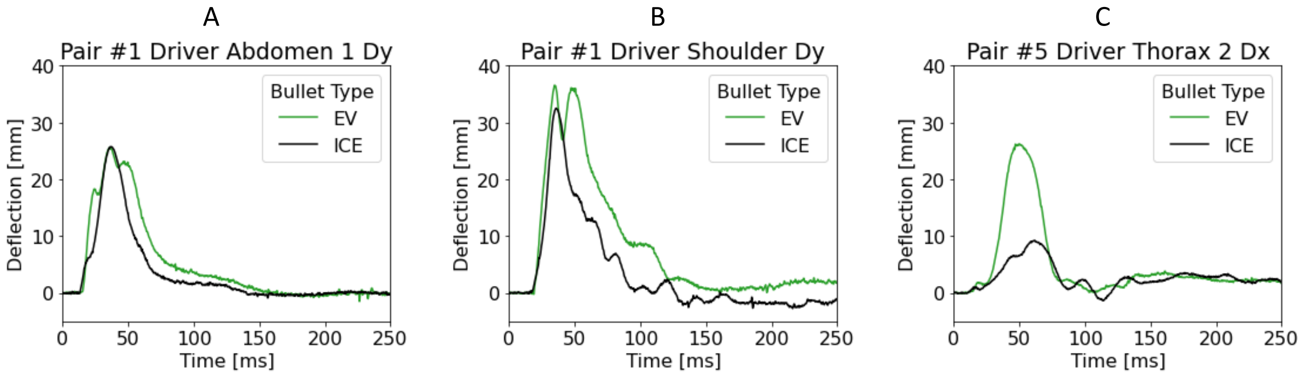

Fig. 6. Example timeseries plots of RibEye deflections measured by the WS-50 with differences in (A, B) lateral deflection peak width and (C) fore-aft deflection.

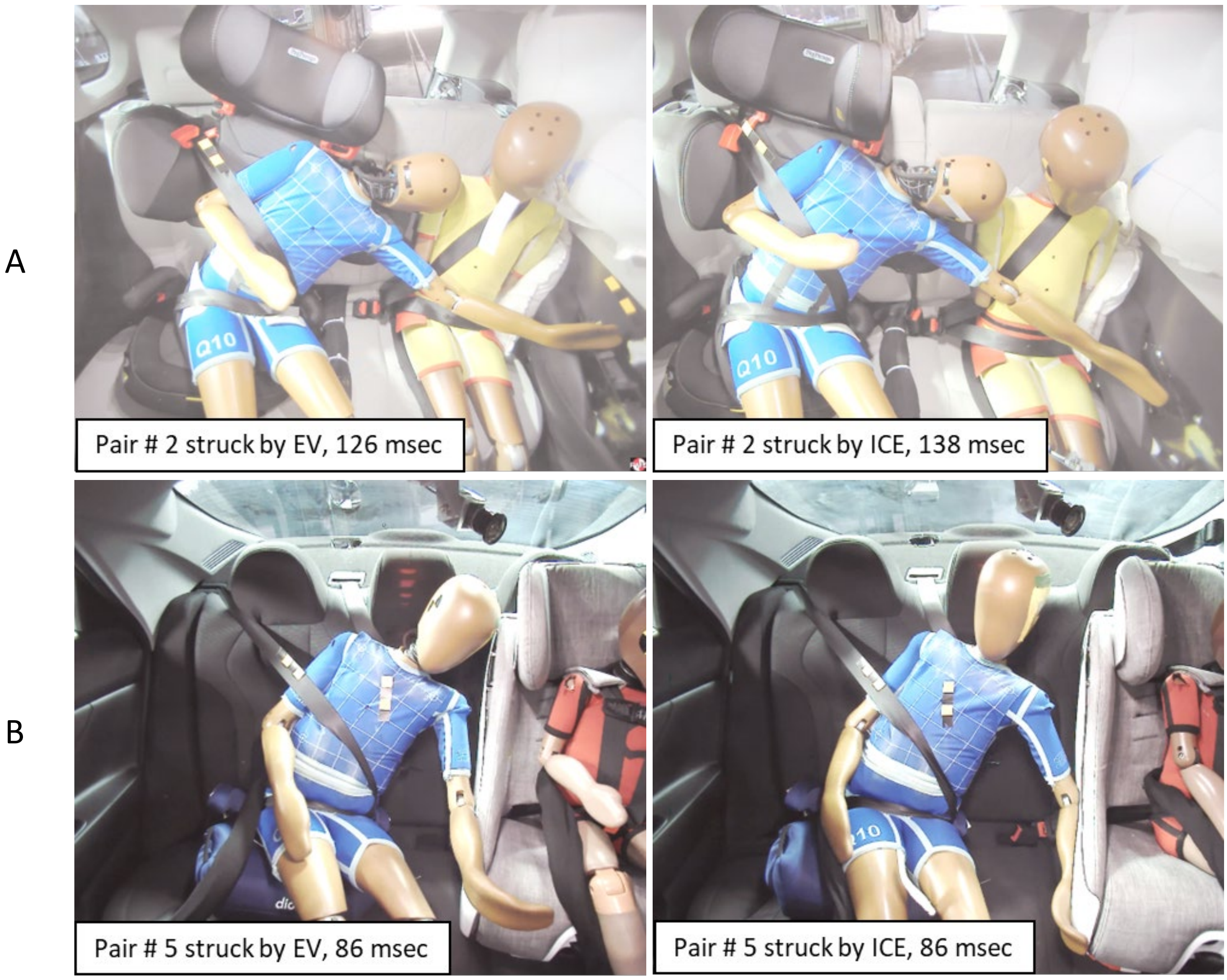

Fig. 7. Comparison of excursions of the Q10 in the right rear seating position in (A) Pair #2 and (B) Pair #5.

Frontal impact

Paired comparison of target vehicle responses

Vehicle pulse characteristics computed from Ax-time responses measured at the target vehicle CG and B pillars are presented in Fig. 8 and the Appendix. Statistically significant mean paired differences are indicated by an asterisk (*), while NS indicates that the mean paired difference was not statistically significant. After applying the Holm-Bonferroni correction for multiple comparisons, delta Vs and average accelerations at the two B pillars as well as peak Ax measured at the vehicle CG were statistically significantly greater for vehicles struck by EVs than for those struck by non-EV bullets.

Median paired differences in ATD kinematic responses in target vehicles

Paired differences in peak head, shoulder, thorax, abdomen, and pelvis kinematic responses were computed for each matched pair of ATDs. Results for the ATDs in the first- and second-row seats are shown in Fig. 9 (results for the ATDs in third-row seats in Pair #8 are in the Appendix). A positive difference indicates that the response was greater in the vehicle struck by the EV than in the vehicle struck by the non-EV. The grey shaded region in Fig. 9 indicates paired differences ≤ 5 g or ≤ 5 mm in magnitude, which were considered to be within the range of repeatability. Markers outside the grey shaded region are annotated according to pair number. The red vertical lines indicate the median paired difference in response.

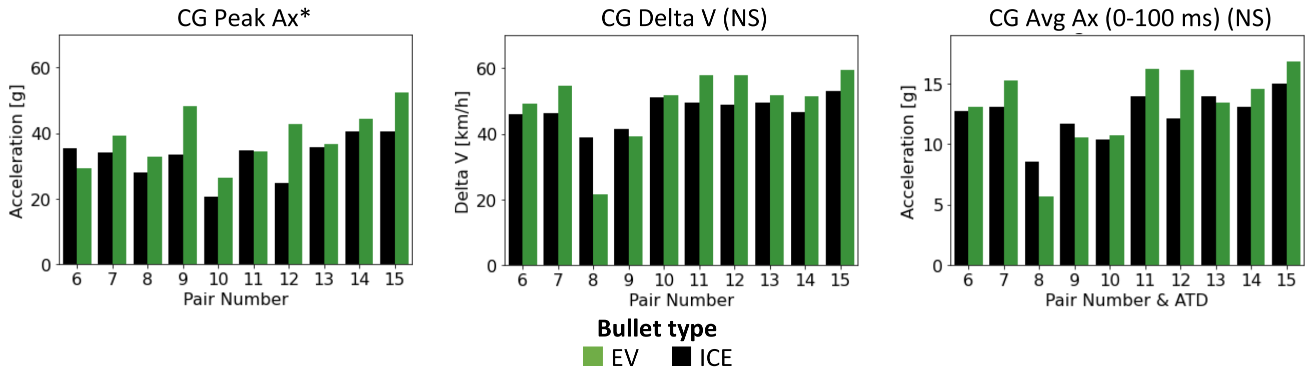

Fig. 8. Vehicle pulse characteristics computed from fore-aft accelerations measured at the vehicle CG.

Overall, median paired differences (Fig. 9, red vertical lines) were within the range of repeatability (Fig. 9, grey shaded region). Specifically, in the first-row seating positions (Fig. 9A-B), the second-row left seating position (Fig. 9C), and the third-row seating positions (Appendix), all median paired differences, except head 3 ms clips of the driver and second-row left passenger, were within the range of repeatability. The second-row right outboard seat (Fig. 9D) was the only location for which the median paired difference in any response other than the head exceeded the range of repeatability. In this seating position, head 3 ms clips, chest 3 ms clips, and peak pelvis Ar were greater in vehicles struck by EV than in vehicles struck by ICE (median paired differences of 8 g, 8 g, and 7 g, respectively). There were no instances of head contacts with either the vehicle interior or the adjacent ATD that resulted in head 3 ms clips ≥80 g.

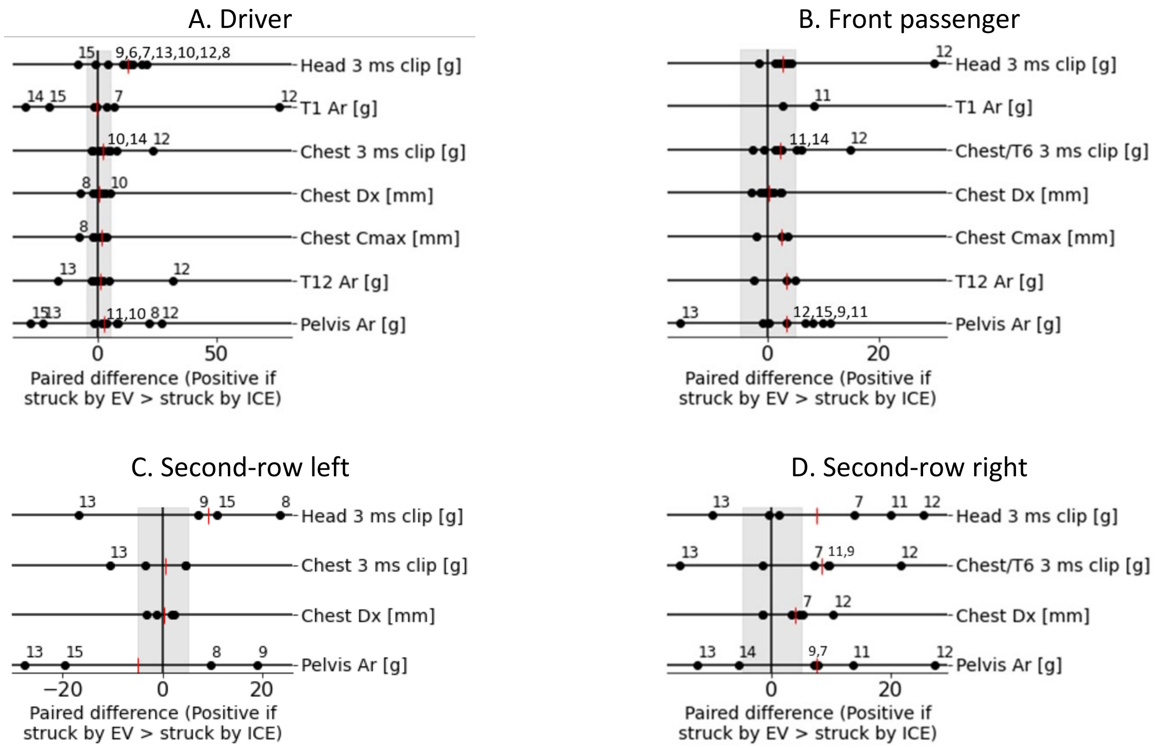

Fig. 9. Paired differences in peak kinematic responses of the ATDs in the target vehicles. Ar = resultant acceleration, Dx = fore-aft deflection.

Examination of individual paired differences in target vehicles

When examining individual matched pairs of ATDs, responses were greater in the vehicle struck by the EV in some pairs, but were greater in the vehicle struck by the non-EV bullet in other pairs. For example, for all matched pairs of ATDs in Pair #12, head 3 ms clips, chest 3 ms clips, and peak pelvis resultant accelerations were greater in the vehicle struck by the EV than in the vehicle struck by the non-EV bullet. By contrast, in Pair #13, ATD responses in all seating positions were overall greater in the vehicle struck by the ICE bullet. Specifically, paired differences exceeding the range of repeatability were observed in all seating positions, and, in all but one case (the TH-50 driver head 3 ms clip), the response was greater in the vehicle struck by the ICE bullet.

IV. DISCUSSION

The objective of this study was to investigate occupant protection in ICE target vehicles in frontal and side impact moving car-to-car tests where the bullet vehicle is an EV or an equivalent model non-EV. Five pairs of side impact tests and ten pairs of frontal offset tests were conducted.

The target vehicles selected were chosen to reflect the mix of vehicles typically seen on Canadian roadways and therefore included a mix of model types (SUV, crossover, sedan, and minivan), fabrication dates, and accrued mileage. The EV bullets were generally newer models; non-EV bullets were a mix of older and newer vehicles.

In the side impact tests, The EV bullet-ICE bullet mass difference for the side impact sample ranged from 334 kg to 821 kg. Vehicle pulse characteristics were greater for target vehicles struck by EVs than for those struck by ICE bullets, while differences in sill beam deformation were mixed. Linear regression models used in [16] to model stiffness metrics of EVs and ICE vehicles as a function of vehicle shadow were reported to have low R^2 values, suggesting high variability of stiffness metrics for both vehicle powertrains. Based on comparisons of stiffness metrics, EVs were reported in [16] to not be “excessively aggressive” compared to ICE vehicles.

ATD responses in the target vehicles of the side impacts were overall slightly greater when struck by an EV than when struck by an ICE bullet. All median paired differences were either within the range of repeatability or indicated that the response was greater in the vehicle struck by the EV. Pair #3 had the smallest difference in mass between EV and ICE bullets and also the fewest paired differences exceeding the range of repeatability. In the other pairs, the variability of individual paired differences was high. For example, in Pair #2 and Pair #4, paired differences exceeding the range of repeatability were measured in the driver T4, T12, and pelvis accelerations, while paired differences in thoracic rib deflection were within the range of repeatability. The inverse was observed in Pair #5: paired differences in thoracic rib deflections exceeded the range of repeatability, whereas paired differences in T4, T12, and pelvis accelerations were within or near the range of repeatability. The paired differences in driver response also did not appear to correlate well with differences in sill beam deformation. For example, paired differences in driver pelvis acceleration were similar in Pair #2 (24 g) and Pair #4 (23 g), but a difference in sill beam deformation forward of the B pillar was observed only for Pair #2. Although not investigated in this study, variability in door trim geometry, side airbag timing, and side airbag geometry between different target vehicle models may contribute to the variability observed in individual paired differences. Because cameras had to be placed away from the intrusion zone, it was not possible to capture the interaction between door trim, side airbag, and ATD.

Injury metrics were generally below IARVs and regulatory limits. At the same time, the injury metrics computed, which were primarily based on peak lateral kinematic and kinetic responses, did not always capture the differences observed in ATD response. For example, in Pair #1, the WS-50 driver RibEye deflections had differences in peak width but not peak magnitude as a function of bullet vehicle type. In Pair #5, RibEye fore-aft deflection varied as a function of bullet vehicle type. A better understanding of the relationship between loading mechanisms and the temporal features of the ATD responses could help to complement current injury metrics.

For the front passenger WS-50, some instances of head contact with the driver were observed, but all head 3 ms clips were below 80 g. The front passenger seat was always aligned with the driver seat. The interactions between the front-row ATDs and the vehicle seats may be different if the front-row seats were not aligned. In the right rear seat, the head 3 ms clip of the Q10 was influenced by both bullet vehicle type and the presence of a CRS in the adjacent struck-side seat. Head contact of the far-side Q10 on the struck-side CRS was always associated with a head 3 ms clip over 80 g, regardless of bullet vehicle powertrain. The difference in head 3 ms clip between cases of Q10 head contact on a CRS (115 ± 13 g) and cases of no CRS contact (36 ± 9 g) was greater than any paired difference in head 3 ms clip measured in the right rear seating position (up to 29 g in magnitude).

Paired differences in far-side Q10 excursion as a function of bullet vehicle type were also qualitatively observed (Fig. 7). In Pair #2, the Q10 reached peak excursion earlier in the vehicle struck by the EV than in the vehicle struck by the ICE bullet. In Pair #5, the Q10 contacted the CRS on the struck side earlier in the vehicle struck by the EV. In the two examples, the far-side Q10 reached peak excursion earlier in the vehicles struck by EV than in those struck by ICE. This was consistent with the vehicle acceleration responses, which were greater for vehicles struck by an EV than those struck by an ICE bullet. These observations suggest that if the far-side occupant head contacts an occupant or CRS in an adjacent seating position, the impact may be more severe when the bullet is an EV.

In the frontal offset tests, target vehicle acceleration responses were on average greater when struck by an EV bullet than when struck by a non-EV bullet. For the ATDs in the target vehicles, however, median paired differences were overall within the range of repeatability. ATD responses in some matched pairs were greater in the vehicle struck by the EV, while in other matched pairs, responses were greater in the vehicle struck by the non-EV; this divergence was observed for all seating locations. Accordingly, bullet vehicle type alone cannot account for the range of paired differences in ATD response measured in the frontal offset test sample.

For the frontal offset sample, the mass difference between an EV bullet and its non-EV counterpart ranged from 177 kg to 617 kg. In a study [16] of 14 EVs and 92 ICE vehicles (all ranging from small cars to large SUVs), EV SUVs were on average 286 kg heavier than ICE SUVs, and EV cars were on average 369 kg heavier than ICE counterparts. For six of the ten pairs of frontal offset tests in this study, the mass difference between the EV bullet and the non-EV bullet was below the mean difference reported in [16]. For pairs with smaller mass differences between EV and non-EV bullets, characteristics of the target and bullet vehicles other than mass may have influenced the difference in ATD response (or lack thereof) measured in the target vehicle. Even in pairs with larger mass differences between EV and non-EV bullets, ATD responses were not necessarily greater in the vehicle struck by the EV. In Pair #15, for example, the EV bullet was 473 kg heavier than the ICE bullet, but the responses of the driver TH-50 were greater in the vehicle struck by the ICE bullet.

In [15], increased bullet vehicle mass, higher bullet vehicle CG, and greater bullet vehicle stiffness metrics were found to be associated with greater odds of injury in the target vehicle of front-to-front crashes. The study was designed to evaluate partner protection metrics while considering mass differences. The sample investigated was mixed and did not specifically distinguish between powertrains. Therefore, the effect of mass in an ICE-to-ICE test could be different from the effect of mass in an EV-to-ICE test.

In this study, two moving vehicle-to-moving vehicle crash configurations were investigated: a side impact test with the bullet and target vehicles travelling perpendicularly to each other and a collinear frontal 40% offset test. For both crash configurations, individual paired differences in ATD response were highly varied. The effect of bullet vehicle type on ATD responses in the target vehicles may be different for other crash configurations. However, given that the reported stiffness characteristics of EVs and ICE vehicles [15],[16] also appeared to be scattered, the high variability of responses observed in this study may also be present in other crash configurations. Parametric analyses conducted using finite element models could be useful to systematically investigate potential sources of the variability observed in this study. They may, for example, aid in determining whether any characteristics of the bullet vehicle other than powertrain and mass could explain the paired differences in ATD response in the target vehicles.

Limitations present in this study included the selection of ICE bullet vehicles and the analysis of the 3D scans. When crash testing for this study began, many EVs entering the market had ICE equivalent models. However, as newer models were introduced, the number of EVs with an equivalent ICE model declined. Therefore, for some pairs, alternative ICE bullets had to be found, which may have added variability to an already small sample. The analysis of the 3D scans of the vehicles was limited by the capabilities of the available software. For example, quantitative analysis of the displacement could not be conducted. Because the rear doors had not been removed for pre-test scanning, there were gaps in the B-pillar data. As a result, the sill was the most reliable surface for analysis. The scanning procedure remains under development.

V. CONCLUSION

In this sample of paired side impact tests, struck-side ATD responses in the target vehicles tended to have slightly greater peak kinematic responses when struck by an EV than when struck by an ICE bullet; however, the injury metrics differed from pair and to pair and were generally below IARVs. On the far side, ATD head responses were influenced by both bullet vehicle type and the struck-side occupant. In frontal offset tests, results were mixed. The high variability of individual paired differences in both crash configurations suggested that differences in bullet vehicle powertrain alone did not account for the range of paired differences observed.

VI. ACKNOWLEDGEMENTS

The authors gratefully acknowledge the staff at PMG Technologies (Blainville, Quebec, Canada) for conducting the tests.

VII. DISCLAIMER

This paper shall not be construed as endorsement, warranty, or guarantee, expressed or implied, on the part of Transport Canada for any evaluated material, product, system or service described herein. Readers should not infer that Transport Canada's evaluation is for any purpose or characteristic other than as stated herein. All information in this document is for information purposes only, and is not intended to provide any specific advice. Any reliance on or use of the information contained in this document is at the user's sole risk and expense.

VIII. FAIR STATEMENT AND DATA AVAILABILITY DECLARATION

The data presented in this study are stored in the Transport Canada crash test database. The tests are assigned unique identifiers, are findable by the associated metadata, and are retrievable by identifier. The metadata are searchable and are stored in a human- and machine-readable format. The data are available upon reasonable request, subject to restrictions such as those associated with privacy, confidentiality, and security.

IX. REFERENCES

[1] Tylko, S., Tang, K., Bussières, A. (2019) Comparison of Occupant Protection in Electric vs. Internal Combustion Vehicles. *Proceedings of IRCOBI Conference*, 2019, Florence, Italy.

[2] Arbelaez, R. A. "As heavy EVs proliferate, their weight may be a drag on safety", www.iihs.org/news/detail/as-heavy-evs-proliferate-their-weight-may-be-a-drag-on-safety. [2026 March 31].

[3] Evans, L. (1984) Driver fatalities versus car mass using a new exposure approach. Accid Anal Prev, **16**(1): p.19-36.

[4] Mizuno, K., Yonezawa, H., (1996) The Effect of Vehicle Mass in Car-to-Car Collisions. SAE Technical Paper 960441.

[5] Frei, P., Kaeser, R. et al. (1997) Crashworthiness and Compatibility of Low Mass Vehicles in Collisions. SAE Technical Paper 970122.

[6] Lund, A., Chapline, J. (1999) Potential Strategies for Improving Crash Compatibility in the U.S. Vehicle Fleet. SAE Technical Paper 1999-01-0066.

[7] Van der Sluis, J. (2000) SWOV Institute for Road Safety Research, *Vehicle compatibility in car-to-car collisions*, Leidschendam, The Netherlands.

[8] Nusholtz, G. S., Rabbiolo, G., Shi, Y. (2003) Estimation of the effects of vehicle size and mass on crash-injury outcome through parameterised probability manifolds. SAE Technical Paper 2003-01-0905.

[9] Hollowell, W. T., Gabler, H. C. (1996) NHTSA's Vehicle Aggressivity and Compatibility Research Program. *Proceedings of ESV Conference*, 1996, Melbourne, Australia.

[10] Summers, S. M., Hollowell, W. T., Prasad, A. (2003) NHTSA's research program for vehicle compatibility. *Proceedings of ESV Conference*, 2003, Nagoya, Japan.

[11] Baker, B. C., Nolan, J. M., O'Neill, B., Genetos, A. P. (2008) Crash compatibility between cars and light trucks: Benefits of lowering front-end energy-absorbing structure in SUVs and pickups. Accid Anal Prev, **40**(1): p.116-125.

[12] Tolouei, R., Maher, M., Titheridge, H. (2013) Vehicle mass and injury risk in two-car crashes: A novel methodology. Accid Anal Prev, **50**: p.155-66.

[13] Monfort, S., Nolan, J. (2019) Trends in aggressivity and driver risk for cars, SUVs, and pickups: Vehicle incompatibility from 1986 to 2016. Traffic Inj Prev, **20**(sup1): p.S92–S96.

[14] Transport Canada. "Memorandum of Understanding (MOU) on Vehicle Compatibility", https://tc.canada.ca/en/road-transportation/motor-vehicle-safety/memorandum-understanding-mou-vehicle-compatibility. [2026 March 31].

[15] Brumbelow, M. L. (2025) Vehicle Design Parameters that Affect Partner Protection in Front-to-Front and Front-to-Side Crashes. *Proceedings of IRCOBI Conference*, 2025, Vilnius, Lithuania.

[16] Mueller, B. C., Brumbelow, M. L., Bragg, H., Jermakian, J. S. (2024) Comparison of frontal crash compatibility

metrics between battery-electric and internal-combustion-engine passenger vehicles. Traffic Inj Prev, **25**(5): p.750-756.

[17] SAE International. (2022), *J211/202208 - Instrumentation for Impact Test.*

[18] Tang, K., Tylko, S., Bussières, A. (2021) Responses of the Hybrid III 5th percentile ATD tested outside of regulatory protocols. *Proceedings of IRCOBI Conference*, 2021, Online.

[19] Virtanen, P., Gommers, R. et al. (2020). SciPy 1.0: Fundamental Algorithms for Scientific Computing in Python. Nature Methods, **17**(3): p.261-272.

[20] Holm, S. (1979) A simple sequentially rejective multiple test procedure. Scandinavian Journal of Statistics, **6**(2): p.65–70.

[21] Poplin, G. S., McMurry, T. L. et al. (2017) Development of thoracic injury risk functions for the THOR ATD. Accid Anal Prev, **106**: p.122-130.

[22] Mertz, H. J., Irwin, A. L., Prasad, P. (2016) Biomechanical and Scaling Basis for Frontal and Side Impact Injury Assessment Reference Values. Stapp Car Crash J, **60**: p.625-657.

X. APPENDIX

Side impact Frontal offset

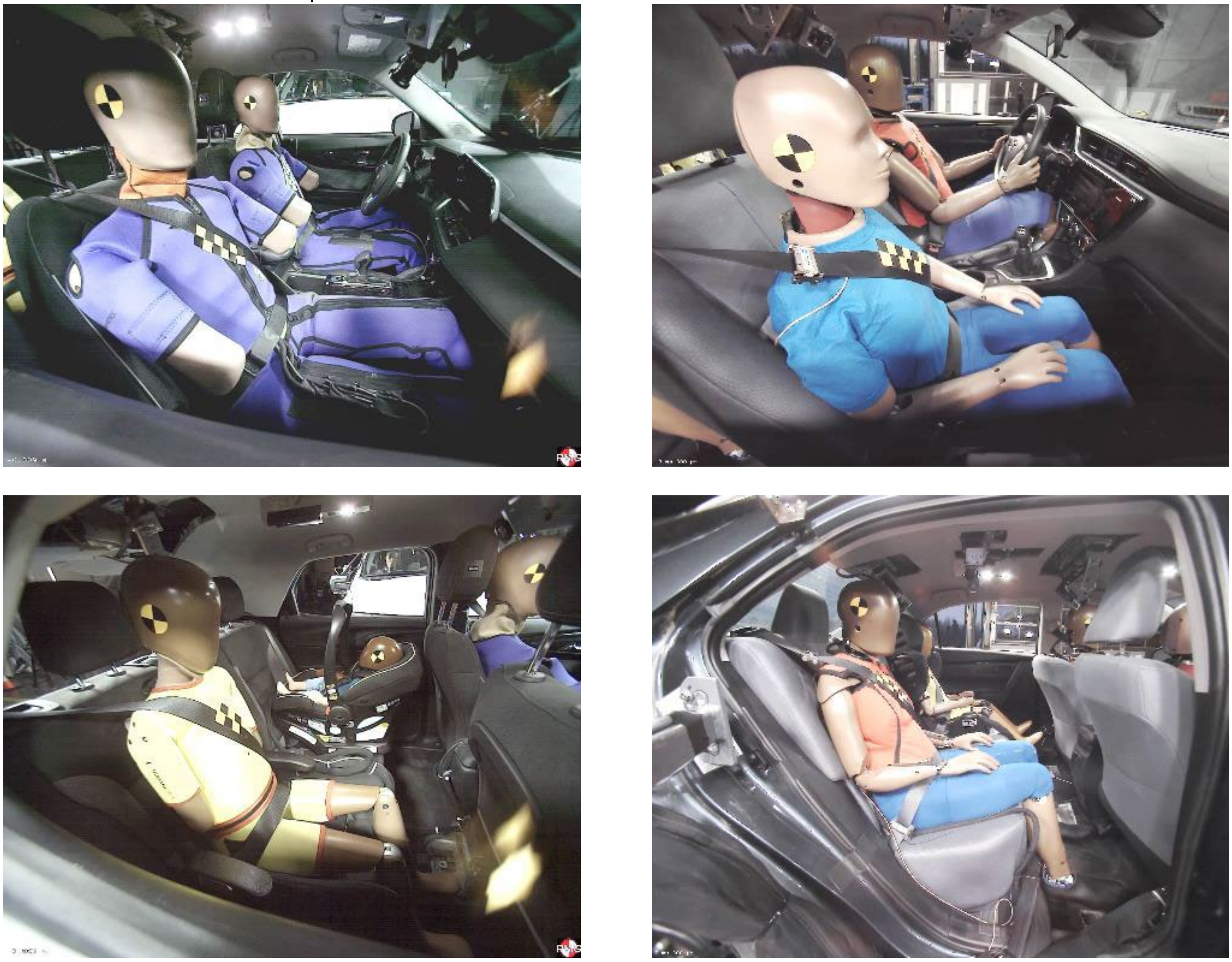

Fig. A 1. Example freeze frames taken at t=0 showing front-row ATDs (top row) and second-row ATDs (bottom row) installed in target vehicles in side impact tests (left column) and frontal offset tests (right column).

TABLE A I
LIST OF WS-50 INSTRUMENTATION AND ASSOCIATED IARVS.

Instrumentation	Injury Metric	IARV
Head CG Accelerometer		
Head CG Angular Rate Sensor		
Neck Load Cell (Upper, Lower)		
Shoulder Left Load Cell	Peak lateral force	4000 N
T1 Accelerometer		
T4 Accelerometer	Peak resultant acceleration	60 g
T12 Accelerometer		
Shoulder RibEye or IR-TRACC	Peak lateral deflection	75 mm
Thorax RibEye or IR-TRACC (Thorax 1, Thorax 2, Thorax 3)	Peak lateral deflection	42 mm
Abdomen RibEye or IR-TRACC (Abdomen 1, Abdomen 2)	Peak lateral deflection	39 mm
Thorax Angular Rate Sensor		
Lumbar Load Cell		
Pelvis Accelerometer	Peak lateral acceleration	130 g
Pelvis Angular Rate Sensor		
Pubic Load Cell	Peak lateral load	6000 N
Sacroiliac Load Cell (Left, Right)	Peak lateral load	6000 N
Femur Acetabulum Load Cell (Left, Right)		

TABLE A II

LIST OF Q10 INSTRUMENTATION AND SIDE IMPACT IARVS. FX = FORE-AFT FORCE, MY = MOMENT ABOUT Y.

Instrumentation	Side Impact Injury Metric	IARV
Head CG Accelerometer		
Head CG Angular Rate Sensor		
Upper Neck Load Cell		
Lower Neck Load Cell		
Chest Accelerometer	Peak resultant acceleration	82 g
Chest Angular Rate Sensor		
Chest IR-TRACC (Upper, Lower)	Peak lateral deflection	30 mm
T1 Accelerometer		
Abdominal Pressure Twin Sensors (frontal impact only)		
Lumbar Load Cell		
Pelvis Accelerometer	Peak lateral acceleration	180 g
Pelvis Angular Rate Sensor		
Sacroiliac Load Cell (Left, Right, Fx and My only)		

TABLE A III

LIST OF Q3S INSTRUMENTATION AND SIDE IMPACT IARVS.

Instrumentation	Side Impact Injury Metric	IARV
Head CG Accelerometer		
Chest Accelerometer	Peak resultant acceleration	92 g
Chest IR-TRACC	Peak lateral deflection	23 mm
Pelvis Accelerometer	Peak lateral acceleration	234 g

TABLE A IV

LIST OF CRABI 12M INSTRUMENTATION AND SIDE IMPACT IARVS.

Instrumentation	Side Impact Injury Metric	IARV
Head CG Accelerometer		
Upper Neck Load Cell		
Chest Accelerometer	Peak resultant acceleration	87 g
Pelvis Accelerometer	Peak lateral acceleration	269 g

TABLE A V

LIST OF HIII 6-YEAR-OLD AND Q6 INSTRUMENTATION.

Instrumentation	HIII 6YO	Q6
Head CG Accelerometer	✓	✓
Neck Load Cell (Upper, Lower)	✓	✓
Chest Accelerometer	✓	✓
Chest Displacement	✓	✓
Chest Angular Rate Sensor	✓*	
Lumbar Load Cell	✓	✓
Iliac Left Load Cell	✓	✓
Iliac Right Load Cell		✓
Pelvis Accelerometer	✓	✓

*Instrumentation not available for all matched pairs

TABLE A VI
LIST OF HIII-50, HIII-05, TH-50, TH-05 INSTRUMENTATION.

Instrumentation	HIII-50	HIII-05	TH-50	TH-05
Head CG Accelerometer	✓	✓	✓	✓
Head CG Angular Rate Sensor	✓*	✓	✓	✓
Head Accelerometer (Top, Side, Rear)			✓	
Upper Neck Load Cell	✓	✓	✓	✓
Lower Neck Load Cell	✓*	✓*	✓	✓
Neck Angle Potentiometer				✓
Skull Spring Load Cell (Front, Rear)			✓	✓
Clavicle Load Cell (Left, Right)		✓*	✓	✓
T1 Accelerometer			✓	✓
Chest/T6 Accelerometer	✓	✓	✓	✓
Spine Accelerometer		✓*		
Sternum Accelerometer				✓
T12 Accelerometer			✓	✓
Chest, T6, or T12 Angular Rate Sensor	✓*		✓	✓
Lumbar Load Cell	✓	✓	✓	
T12 Load Cell				✓
Chest potentiometer	✓	✓		
Thorax RibEye (Ribs 1-6, Left & Right)		✓*		
Thorax IR-TRACC (Upper & Lower, Left & Right)			✓	✓
Abdomen IR-TRACC (Left, Right)			✓	
Upper Abdomen Accelerometer			✓	
Abdominal Pressure Twin Sensors (Left, Right)				✓
Pelvis Accelerometer	✓	✓	✓	✓
Pelvic Angular Rate Sensor			✓	✓
Iliac Load Cell (Left, Right)		✓	✓	✓
Acetabulum Load Cell (Left, Right)			✓	✓
Femur Load Cell (Left, Right)	✓	✓	✓	✓*
Knee Slider Displacement Potentiometer (Left, Right)		✓*	✓	✓*
Tibia Load Cell (Left & Right, Upper & Lower)			✓	✓*
Tibia Accelerometer (Left, Right)			✓	✓*
Achilles Load Cell (Left, Right)			✓	✓*
Ankle Rotation Potentiometer (Left, Right)			✓	✓*
Foot Acceleration (Left, Right)			✓	✓*

*Instrumentation not available for all matched pairs

TABLE A VII

RESULTS OF LINEAR REGRESSION BETWEEN BULLET-TARGET MASS DIFFERENCE AND FRONT-ROW ATD RESPONSES IN THE TARGET VEHICLE IN SIDE IMPACT TESTS.

Seating position	ATD Response [unit]	Maximum measured value	Linear model slope	Linear model R^2
Driver	WS-50 head 3 ms clip [g]	43	0.0148	0.90
Driver	WS-50 peak T1 Ar [g]	46	0.0114	0.47
Driver	WS-50 peak shoulder Dy [mm]	43	0.0161	0.56
Driver	WS-50 peak rib 1 Dy [mm]	29	0.0079	0.27
Driver	WS-50 peak rib 2 Dy [mm]	25	0.0066	0.21
Driver	WS-50 peak rib 3 Dy [mm]	25	0.0094	0.41
Driver	WS-50 peak abdomen 1 Dy [mm]	26	0.0092	0.72
Driver	WS-50 peak abdomen 2 Dy [mm]	46	0.0077	0.16
Driver	WS-50 T4 Ar [g]	41	0.0106	0.63
Driver	WS-50 T12 Ar	46	0.0118	0.48
Driver	WS-50 peak pelvis Ay [g]	62	0.0132	0.41
Front passenger	WS-50 head 3 ms clip [g]	64	0.0214	0.71
Front passenger	WS-50 peak T1 Ar [g]	35	0.0078	0.68
Front passenger	WS-50 peak shoulder Dy [mm]	4	0.0011	0.31
Front passenger	WS-50 peak rib 1 Dy [mm]	4	0.0008	0.23
Front passenger	WS-50 peak rib 2 Dy [mm]	6	0.0022	0.61
Front passenger	WS-50 peak rib 3 Dy [mm]	20	0.0074	0.58
Front passenger	WS-50 peak abdomen 1 Dy [mm]	16	0.0087	0.46
Front passenger	WS-50 peak abdomen 2 Dy [mm]	20	-0.002	0.07
Front passenger	WS-50 T4 Ar [g]	33	0.0082	0.73
Front passenger	WS-50 T12 Ar	39	0.0003	0
Front passenger	WS-50 peak pelvis Ay [g]	42	0.0024	0.09

TABLE A VIII

RESULTS OF LINEAR REGRESSION BETWEEN BULLET-TARGET MASS DIFFERENCE AND FRONT-ROW ATD RESPONSES IN THE TARGET VEHICLE IN FRONTAL OFFSET TESTS.

Seating position	ATD Response [unit]	Linear model slope	Linear model R^2
Driver	Head 3 ms clip [g]	0.0119	0.12
Driver	Head 3 ms clip, TH-50M data only [g]	0.0084	0.06
Driver	Peak T1 Ar [g]	0.0199	0.08
Driver	Chest 3 ms clip [g]	0.0069	0.10
Driver	Chest 3 ms clip, TH-50M data only [g]	0.0051	0.07
Driver	Peak chest Dx [mm]	0.0063	0.03
Driver	Peak chest Dx, TH-50M data only [mm]	0.0115	0.25
Driver	Chest Cmax [mm]	0.0117	0.24
Driver	Peak T12 Ar [g]	0.0046	0.02
Driver	Peak pelvis Ar [g]	0.0140	0.05
Driver	Peak pelvis Ar, TH-50M data only [g]	0.0127	0.05
Front passenger	Head 3 ms clip [g]	0.0128	0.17
Front passenger	Head 3 ms clip, HIII-05F data only [g]	0.0224	0.46
Front passenger	Chest/T6 3 ms clip [g]	0.0096	0.17
Front passenger	Chest 3 ms clip, HIII-05F data only [g]	0.0087	0.26
Front passenger	Peak chest Dx [mm]	0.0316	0.17
Front passenger	Peak chest Dx, HIII-05F data only [g]	0.0022	0.01
Front passenger	Chest Cmax [mm]	0.0113	0.22
Front passenger	Peak T12 Ar [g]	0.0205	0.19
Front passenger	Peak pelvis Ar [g]	0.016	0.16
Front passenger	Peak pelvis Ar, HIII-05F data only [g]	0.0058	0.03

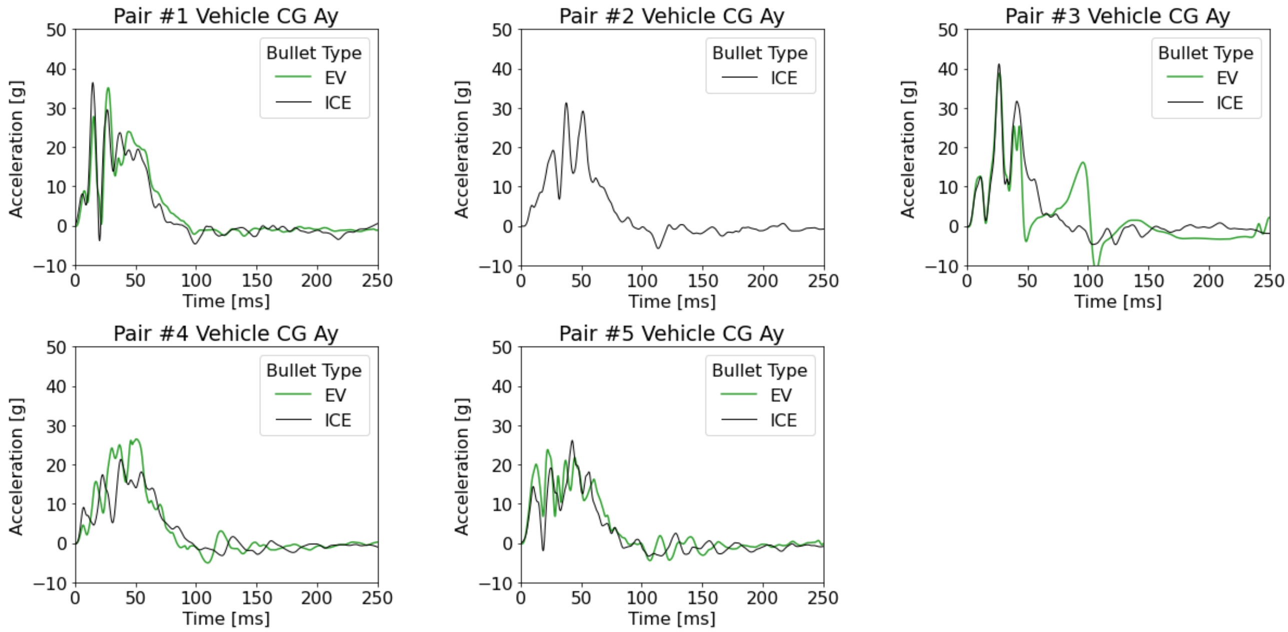

Fig. A 2. Acceleration-time plots of lateral accelerations recorded at target vehicle CGs in the side impacts.

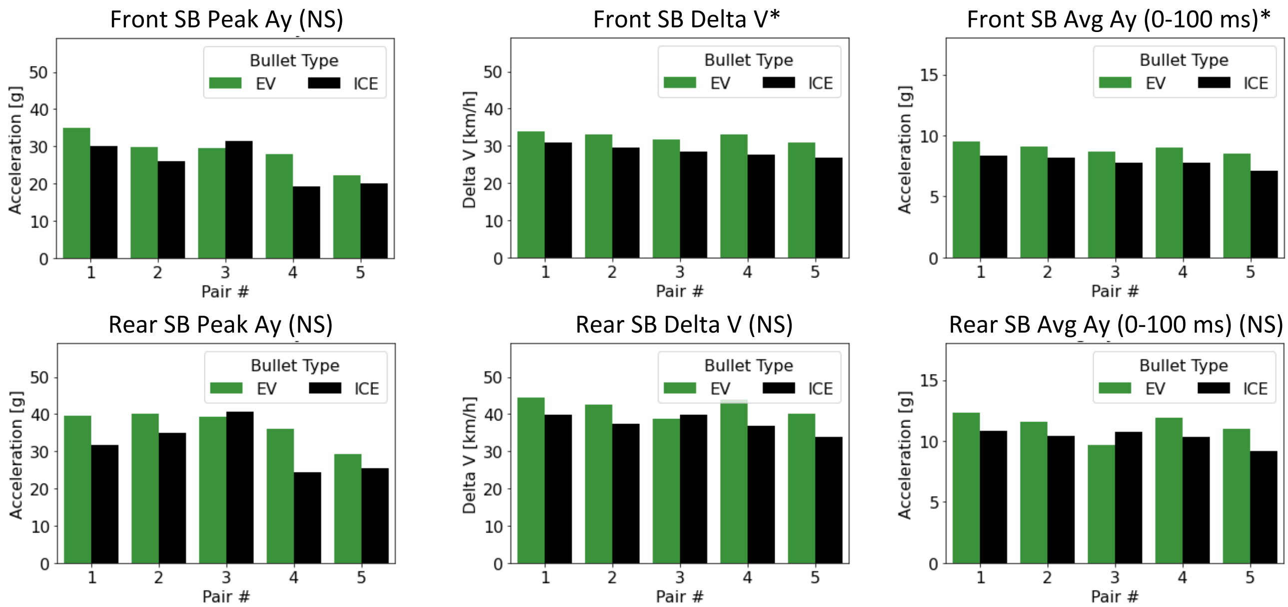

Fig. A 3. Vehicle pulse characteristics of the target vehicles in side impact pairs at the sill beams (SB). Statistically significant mean paired differences are indicated by an asterisk (*), while NS indicates that the mean paired difference was not statistically significant.

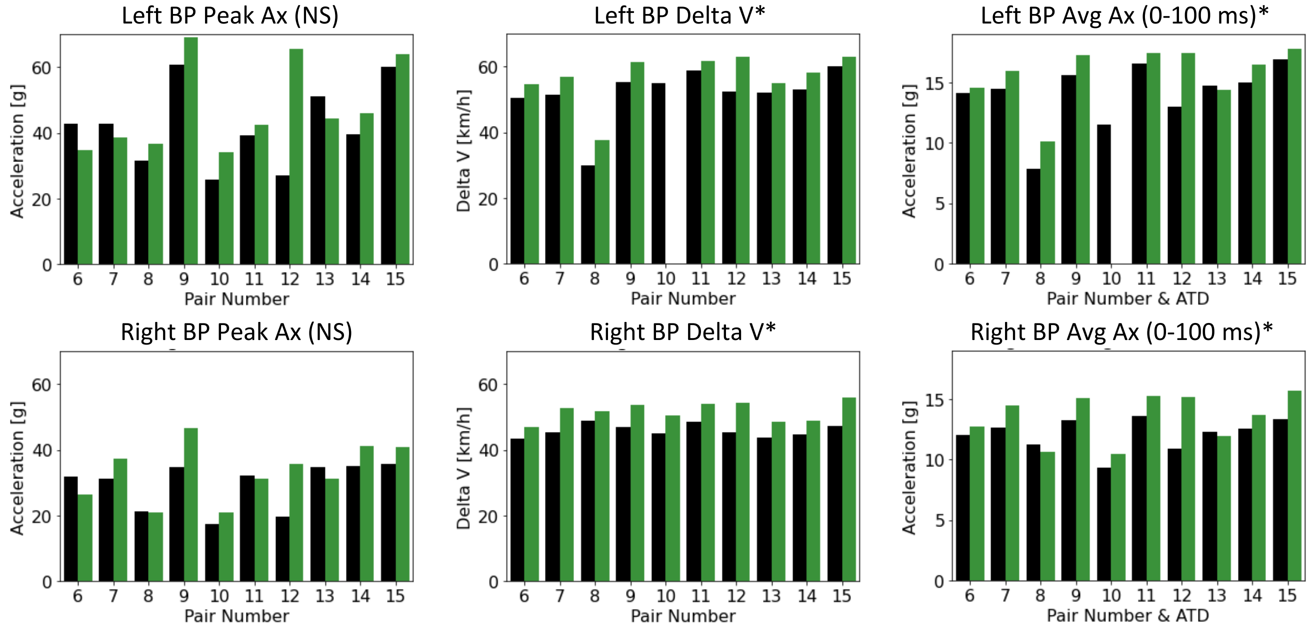

Fig. A 4. Vehicle pulse characteristics of the target vehicles in frontal offset impact pairs. Statistically significant mean paired differences are indicated by an asterisk (*), while NS indicates that the mean paired difference was not statistically significant.

TABLE A IX

PEAK KINEMATIC RESPONSES RECORDED IN THIRD-ROW SEATING POSITIONS IN FRONTAL IMPACTS IN PAIR #8

Seat position (ATD)	**Response [unit]**	**Response in vehicle struck by ICE**	**Response in vehicle struck by EV**	**Difference**
Third row left (Q10)	Head 3 ms clip [g]	55	55	0
	Chest peak Ar [g]	43	44	1
	Chest peak Dx [mm]	47	50	3
	Pelvis peak Ar [g]	42	43	1
Third row right (Q10)	Head 3 ms clip [g]	38	34	-4
	Chest peak Ar [g]	30	33	3
	Chest peak Dx [mm]	36	36	0
	Pelvis peak Ar [g]	83	83	0